Polyhedron 206 (2021) 115298

Contents lists available at ScienceDirect

Polyhedron

journal homepage: www.elsevier.com/locate/poly

Rare nuclearities in Mn/oxo cluster chemistry: Synthesis and characterization of a mixed-valence $\{Mn^{II/III}_{11}\}$ complex bearing acetate and salicylhydroximate(-3) bridging/chelating ligands☆

Evangelia S. Koumousi [a], Gerasimi Lazari [a], Spyridon Grammatikopoulos [a], Constantina Papatriantafyllopoulou [b,c], Manolis J. Manos [d,e], Spyros P. Perlepes [a], Anastasios J. Tasiopoulos [d], George Christou [b], Theocharis C. Stamatatos [a,*]

[a] Department of Chemistry, University of Patras, 265 04 Patras, Greece
[b] Department of Chemistry, University of Florida, Gainesville, 32611-7200 Florida, USA
[c] School of Chemistry, College of Science and Engineering, National University of Ireland Galway, University Road, H91 TK33 Galway, Ireland
[d] Department of Chemistry, University of Cyprus, Nicosia 1678, Cyprus
[e] Department of Chemistry, University of Ioannina, Ioannina 45110, Greece

ARTICLE INFO

Keywords:
Coordination clusters
Manganese
Salicylhydroxamic acid
Undecanuclearity
Magnetochemistry

ABSTRACT

The one-pot reaction between $Mn(O_2CMe)_2{\cdot}4H_2O$, salicylhydroxamic acid ($shaH_2$) and $Me_4NOH{\cdot}5H_2O$ in a molar ratio of 2:1:2, and a solvent mixture comprising MeCN and MeOH, affords the new mixed-valence cluster compound $(Me_4N)_4[Mn^{II}_2Mn^{III}_9O_4(O_2CMe)_9(shi)_6]$ (**1**) in moderate yields. The anion of the tetradentate (N,O,O,O) chelating/bridging ligand shi^{3-} resulted from the in-situ metal ion-assisted amide-iminol tautomerism of $shaH_2$. The $[Mn^{II}_2Mn^{III}_9(\mu_3\text{-}O)_4(\mu\text{-}OR)_3(\mu_3\text{-}NO)_6]^{14+}$ core of **1** comprises four vertex-sharing $\{Mn^{III}_3(\mu_3\text{-}O^{2-})\}^{7+}$ triangular subunits of different types, which are linked to each other and the Mn^{II} atoms through the oximato arms and the carboxylate O-atoms of six $\eta^1{:}\eta^1{:}\eta^1{:}\eta^2{:}\mu_3$ shi^{3-} and three $\eta^1{:}\eta^2{:}\mu_3$ $MeCO_2^-$ groups, respectively. Peripheral ligation about the core is provided by six $\eta^1{:}\eta^1{:}\mu$ $MeCO_2^-$ groups and the chelating parts of the shi^{3-} ligands. Solid-state direct-current (dc) magnetic susceptibility studies revealed the presence of predominant antiferromagnetic exchange interactions between the Mn centers, mainly promoted by the coplanarity of the $\mu_3\text{-}O^{2-}$ within the $\{Mn_3\}$ triangular planes and the insignificant distortion of the Mn—N—O—Mn bridging units. Low-lying excited states precluded obtaining a good fit from the magnetization data, and the ground state was instead determined from the alternating-current (ac) data, which indicated an $S = 3$ ground state for **1**. The combined results emphasize the continuing supply from the use of the salicylhydroxime chelating/bridging ligand of new 3d-metal clusters of very rare nuclearities and beautiful molecular structures.

1. Introduction

Molecular nanoscience has emerged as a cross-disciplinary field of research which is focused on the study of high-nuclearity molecular compounds with nanoscale dimensions and properties akin to bulk materials, such as metals, metal oxides and alloys [1]. One of the major challenges in the field of molecular nanoscience is the employment of the appropriate synthetic conditions for the crystallization and structural characterization of polynuclear metal complexes (or coordination clusters) with unprecedented topologies and interesting physical properties [2]. The choice of the bridging/chelating ligand 'blends' remains to date an important synthetic variable for the isolation of molecular nanoscale complexes of various 3d-, 4f- and/or 3d/4f-metal combinations [3,4,5]. To this end, several organic chelates, such as pyridyl alcohols [6], diols and triols [7], Schiff bases [8], and oximates, such as 2-pyridyl oximes [9], R-substituted salicylaldoximes [10] and pyridyl dioximes [11], have already unveiled their capacity to bridge many metal ions and stabilize nanosized cluster compounds with large nuclearities and beautiful structural motifs. In addition, carboxylates [12], β-diketonates [13] and various pseudohalides [14] have held a key

☆ Part of the Special Issue dedicated to the element manganese, entitled "Manganese: A Tribute to Chemical Diversity".

* Corresponding author.
E-mail address: thstama@upatras.gr (T.C. Stamatatos).

https://doi.org/10.1016/j.poly.2021.115298
Received 15 April 2021; Accepted 26 May 2021
Available online 31 May 2021

role as complementary or -occasionally- primary bridging ligands in the quest for new, high-nuclearity metal clusters.

The coordination chemistry of Mn has long been attracting the interest of many scientific groups in different research fields of chemistry, physics, biology, and materials science. This interest mainly stems from the rich redox activity of Mn, its ability to form high-nuclearity metal-oxo complexes at various oxidation states (II, III, and IV), and the plethora of interesting applications that such molecular species can find as: (i) structural models of different biological metallosites [15], (ii) high-spin molecules and single-molecule magnets (SMMs) [16], (iii) magnetic refrigerants [17], (iv) magneto-optical or multifunctional materials (i.e., ferromagnetic and ferroelectric) [18], and (v) oxidation catalysts [19]. Indeed, the discovery of the gigantic $\{Mn_{84}\}$ [20] and $\{Mn_{70}\}$ [21] torus-like complexes and the $\{Mn_{49}\}$ cuboctahedron [22], all with nanosized dimensions and SMM behavior, has established manganese as one of the leading metals in molecular nanoscience and nanomagnetism.

Our group has had a longstanding success in the synthesis of polynuclear Mn complexes at various oxidation states and mixed-valence descriptions with a wide variety of organic chelates and ancillary carboxylate- or azido-bridging groups [6,9,14,18]. Our long-term objectives are oriented towards the search for new and efficient SMMs, and hybrid magnetic materials exhibiting both SMM and photoluminescence responses [23]. In this direction, Pecoraro and some of us have independently employed salicylhydroxamic acid ($shaH_2$, Scheme 1) as the primary organic chelate for the preparation of many structurally and magnetically interesting homometallic Mn^{n+} [24] and heterometallic Mn/Ca [23,25] and Mn/Ln [26] complexes. The main interest in salicylhydroxamic acid ($shaH_2$) stems from its ability to undergo a metal-assisted amide-iminol tautomerism, which generates *in situ* salicylhydroxime ($shiH_3$; Scheme 1). The latter is a mixed alkoxo-oximato ligand on deprotonation with four available coordination sites, which can potentially chelate and bridge many metal centers. However, the majority of shi^{3-}-based metal complexes belong to the general family of metallacrowns, a class of oxido-free, macrocyclic compounds containing [M—N—O—M] repeating arrays with interesting host–guest and supramolecular properties [27].

In this work, we have incorporated shi^{3-} in Mn oxo-carboxylate chemistry, and from the synthetic 'blend' of $Mn/shaH_2/MeCO_2^-/Me_4NOH$ we were able to isolate, and structurally, spectroscopically, and magnetically characterize the mixed-valence, 0-D cluster $(Me_4N)_4[Mn^{II}_2Mn^{III}_9O_4(O_2CMe)_9(shi)_6]$ (**1**), which inter alia possesses a rare nuclearity and structural topology with nanoscale dimensions of ~2 nm.

2. Experimental

2.1. Materials, general methods, and physical measurements

All manipulations were performed under aerobic conditions using materials (reagent grade) and solvents as received. Infrared (IR) spectra were recorded in the solid state (KBr pellets) on a Nicolet Nexus 670 FTIR spectrometer in the 400–4000 cm^{-1} range. Elemental analyses (C, H, and N) were performed on a Perkin-Elmer 2400 Series II Analyzer. Variable-temperature direct current (dc) and alternating current (ac) magnetic susceptibility data were collected on a Quantum Design MPMS-XL SQUID susceptometer equipped with a 7 T magnet and operating in the 1.8–400 K range. The microcrystalline sample was embedded in solid eicosane to prevent torquing. Ac magnetic susceptibility measurements were performed in an oscillating ac field of 3.5 G, at zero external dc field; the oscillation frequencies were in the 50–1000 Hz range. Pascal's constants were used to estimate the total diamagnetic correction, which was subtracted from the experimental susceptibility to give the molar paramagnetic susceptibilities (χ_M) [28].

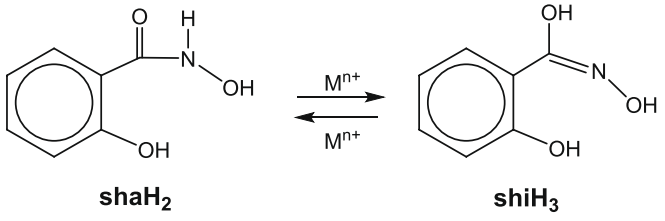

Scheme 1. Metal-assisted amide-iminol tautomerism of $shaH_2$ to $shiH_3$.

2.2. Preparation of complex

2.2.1. $(Me_4N)_4[Mn_{11}O_4(O_2CMe)_9(shi)_6]$ (1)

To a stirred, colorless solution of $shaH_2$ (0.08 g, 0.5 mmol) and $Me_4NOH{\cdot}5H_2O$ (0.18 g, 1.0 mmol) in MeCN (15 mL) was added a pink solution of $Mn(O_2CMe)_2{\cdot}4H_2O$ (0.25 g, 1.0 mmol) in MeOH (5 mL). The resulting dark red solution was stirred for 20 min, during which time a noticeable color change to very dark brown was observed. The solution was filtered, and Et_2O (40 mL) diffused into the filtrate. After two weeks, the resulting dark red plate-like crystals of **1**·3MeCN were collected by filtration, washed with cold MeCN (2 × 3 mL) and Et_2O (2 × 3 mL), and dried under vacuum; the yield was 25% (based on the total available Mn). The vacuum-dried, crystalline solid was satisfactorily analyzed as **1**·$3H_2O$. *Anal.* Calc.: C, 37.24; H, 4.32; N, 5.71%. Found: C, 37.11; H, 4.22; N, 5.92%. Selected IR data (cm^{-1}): 3422 (sb), 3016 (m), 1574 (s), 1518 (m), 1446 (m), 1410 (m), 1314 (m), 1256 (m), 1150 (w), 1104 (w), 1024 (m), 930 (m), 862 (w), 762 (m), 694 (mb), 662 (mb), 540 (w), 404 (w).

2.3. Single-crystal X-ray crystallography

Single-crystal X-ray diffraction data for **1**·3MeCN were collected on a Rigaku Oxford Diffraction Supernova diffractometer, equipped with a CCD area detector utilizing Cu Kα (λ = 1.5418 Å) radiation. A suitable crystal was attached to a glass fiber using paratone-N oil and transferred to goniostat where it was cooled for data collection. Empirical absorption corrections (multiscan based on symmetry-related measurements) were applied using CrysAlis RED software [29]. The same software package was used for data collection, cell refinement, and data reduction. The structure was solved by direct methods using SHELXS [30] through the WinGX interface [31], and it was refined on F^2 using full-matrix least-squares with SHELXL-2018/3 [32] via the ShelXle [33] interface. The non-H atoms were treated anisotropically, whereas the H atoms of MeCN molecules were placed at calculated, ideal positions and refined as riding on their respective carbon atoms. Various figures of the structure were created using the Diamond 3 [34] software package. Unit cell parameters, structure solution and refinement details for **1**·3MeCN are summarized in Table 1. Further crystallographic details can be found in the corresponding CIF file provided in the ESI.

3. Results and discussion

3.1. Synthetic comments

The synthetic route employed for the isolation of high-nuclearity Mn/oxo clusters bearing salicylhydroximate (shi^{3-}) and carboxylate (RCO_2^-) ions as supporting bridging/chelating ligands involved the 2:1:2 reaction between $Mn(O_2CMe)_2{\cdot}4H_2O$, $shaH_2$ and $Me_4NOH{\cdot}5H_2O$ in a solvent mixture comprising MeCN and MeOH. Crystallization of the resulting dark brown filtrate from a slow diffusion with Et_2O has led to the formation of dark red crystals of the mixed-valence cluster compound $(Me_4N)_4[Mn^{II}_2Mn^{III}_9O_4(O_2CMe)_9(shi)_6]$ (**1**) in moderate yields (~25% based on the total available Mn). The formation of **1** is summarized in the balanced Eq. (1).

Table 1
Crystallographic data for complex **1**·3MeCN.

Parameter	**1**·3MeCN
Empirical formula	$C_{82}H_{108}Mn_{11}N_{13}O_{40}$
FW/g mol^{-1}	2520.16
Temperature/K	100(2)
Crystal type	Dark-red polyhedral
Crystal size/mm^3	0.10 × 0.08 × 0.07
Crystal system	Cubic
Space group	$P2_13$
a/Å	23.1888(3)
Volume/Å^3	12469.1(5)
Z	4
ρ_{calc}/g cm^{-3}	1.342
μ/mm^{-1}	9.382
θ (°)	6.33 to 61.44
F(000)	5144
Radiation	Cu Kα ($\lambda = 1.54184$)
Index ranges	$-26 \le h \le 26$ $-26 \le k \le 26$ $-23 \le l \le 26$
Reflections collected (R_{int})	51649 (0.0616)
Data/restraints/parameters	6426/0/441
Goodness-of-fit on F^2	1.013
Final R indexes [$I \ge 2\sigma(I)$] [a,b]	$R_1 = 0.0352$ w$R_2 = 0.0885$
Final R indexes [all data]	$R_1 = 0.0471$ w$R_2 = 0.0933$
$(\Delta\rho)_{max,min}$/e Å^{-3}	0.435 and −0.231

[a] $R_1 = \Sigma(||F_o| - |F_c||)/\Sigma|F_o|$.
[b] $wR_2 = [\Sigma[w(F_o^2 - F_c^2)^2]/\Sigma[w(F_o^2)^2]]^{1/2}$, $w = 1/[\sigma^2(F_o^2) + (ap)^2 + bp]$, where $p = [\max(F_o^2, 0) + 2F_c^2]/3$.

$$Mn(O_2CMe)_2 + 6\ shiH_3 + 9/4\ O_2 + 17\ Me_4NOH \rightarrow (Me_4N)_4[Mn_{11}O_4(O_2CMe)_9(shi)_6] + 13\ (Me_4N)(O_2CMe) + 35/2\ H_2O \quad (1)$$

The coordinated shi^{3-} groups resulted from the metal ion-assisted transformation of $shaH_2$ under the reported synthetic conditions (Scheme 1). Adjustment of the experimental molar ratios of the precursors [Mn(O$_2$CMe)$_2$:shiH$_3$:Me$_4$NOH = 2:1:2] to the stoichiometric equivalents [Mn(O$_2$CMe)$_2$:shiH$_3$:Me$_4$NOH = 11:6:17 ~ 2:1:3], in an attempt to optimize the isolated yields of **1**, failed to reproduce the crystals of the same cluster compound **1**. The MeCN/MeOH reaction solvent mixture was identified as the one giving the highest product yield and purity, as well as the best quality single crystals. When MeOH was excluded from the reaction mixture, the progress of the reaction was retarded due to the poor solubility of Mn(O$_2$CMe)$_2$·4H$_2$O in MeCN and longer stirring times were required to eventually obtain a dark brown solution. The crystallization of the latter filtrate was successful in yielding crystals of **1**, but the crystals were always contaminated with white solids as byproducts.

The synthesis of **1** involves Mn oxidation, undoubtedly by O$_2$ under the prevailing basic conditions, and Eq. (1) has been balanced accordingly. The base Me$_4$NOH is essential for the pure synthesis of the crystalline complex **1**. Importantly, it facilitates the deprotonation of the $shaH_2$/shiH$_3$ ligands and subsequently generates Me$_4$N$^+$ cations in solution, which were found to participate as countercations for the stabilization of the anionic, 0-D cluster **1** in the solid-state (*vide infra*). Employment of different organic bases, such as NMe$_3$, NEt$_3$, NBu$^n_3$, Et$_4$NOH and Bu$^n_4$NOH, under the exact same conditions, did not afford crystalline materials but only oily products that we were not able to further characterize. It is very likely that the basicity of the employed base and/or the stereochemical ability of the corresponding cations (i.e., Me$_3$NH$^+$, Et$_3$NH$^+$, Et$_4$N$^+$, and so on) to counterbalance high-nuclearity Mn/shi^{3-} clusters have a pronounced effect on the stabilization and crystallization of the reported complex **1**. To this end, Pecoraro, Tegoni and coworkers have recently reported a structurally similar to **1** cluster compound, which was counterbalanced by four Na$^+$ cations, as a result of the employment of NaO$_2$CMe in the reaction mixture and the absence of an external organic base [35]. The previously reported Na$_4$[Mn$_{11}$O$_4$(O$_2$CMe)$_9$(shi)$_6$(DMF)$_3$] compound exhibits a three-dimensional supramolecular structure, resulted from the coordination of the Na$^+$ atoms with the carboxylate O atoms and the DMF solvate molecules. No magnetic study has been reported for the 3-D {Mn$_{11}$} complex.

3.2. Description of structure

The crystal structure of **1** consists of [Mn$_{11}$O$_4$(O$_2$CMe)$_9$(shi)$_6$]$^{4-}$ anions (Fig. 1) counterbalanced by Me$_4$N$^+$ cations. In addition, there are three MeCN solvent molecules in the crystal lattice, which are weakly interacting with the cluster compound, and they will not be further discussed. Selected interatomic distances and angles of **1** are listed in Table 2. The formula of **1** is based on metric parameters, charge-balance considerations, and bond valence sum (BVS) calculations on the Mn and selected O atoms (Table 3).

The anionic cage-like cluster [Mn$_{11}$O$_4$(O$_2$CMe)$_9$(shi)$_6$]$^{4-}$ is built around a C_3-axis which includes the crystallographically unique Mn1, Mn5 and O8 atoms. The latter O^{2-} ion (O8) is μ$_3$-bridged to Mn3 and its symmetry-related partners (Mn3′ and Mn3″) to give an ideal equilateral triangle (type **A**) positioned perpendicular to the C_3-axis and featuring Mn···Mn separations of 3.215(1) Å and Mn-O8-Mn angles of 120° (Fig. 2, left). Furthermore, three equivalent by symmetry {Mn$^{III}_3$O(O$_2$CMe)$_3$(shi)$_2$}$^{2-}$ triangular subunits (type **B**), comprising Mn2, Mn3 and Mn4 atoms, are generated by the 3-fold axis and linked to the divalent Mn1 and Mn2 through the alkoxido- (O1, O4) and oximato- (O2, O5) oxygen atoms of the shi^{3-} ligands (Fig. 2, right). The three edges, Mn2···Mn3, Mn3···Mn4 and Mn4···Mn2, of each triangle are bridged by an $\eta^1{:}\eta^1$:μ-MeCO$_2^-$ ion and a μ-NO$^-$ group from an $\eta^1{:}\eta^1{:}\eta^1{:}\eta^2$:μ$_3$ shi^{3-} ligand, an oximato group from a different unsupported $\eta^1{:}\eta^1{:}\eta^1{:}\eta^2$:μ$_3$ shi^{3-} ligand, and two $\eta^1{:}\eta^1$:μ-MeCO$_2^-$ groups, respectively. The Mn···Mn separations within type **B** triangles differ from each other (3.142(1)-3.327(1) Å); these triangles are thus scalene.

The central, μ$_3$-bridging oxide ion, O7, of each triangle **B** is only 0.062 Å above the Mn$_3$ plane, pointed towards the unsupported shi^{3-} ligand, and the three Mn-O^{2-} bonds are similar (1.854(4)-1.871(4) Å) and comparable with those reported for discrete complexes containing the [Mn$^{III}_3$(μ$_3$-O)(μ-O$_2$CR)$_x$(μ-NO)$_y$]$^{n+}$ core (R = various; x, y, n ≥ 1) [36]. The Mn-O^{2-}-Mn angles span the range 114.4(2)-126.5(2)°. The diatomic oximato group of the unsupported shi^{3-} ligand is noticeably twisted, as reflected in the torsion angle about the N—O bond of 21.2(4)°, whereas the Mn—N—O—Mn torsion angle of the shi^{3-}/MeCO$_2^-$ triangular edge is only 3.2(4)°. The combined structural features in Mn^{III}-containing clusters bearing oxido/carboxylate/oximato bridges have been found to significantly affect their magnetic response. A combination of a planar {Mn$_3$(μ$_3$-O^{2-})}$^{7+}$ core and a small Mn—N—O—Mn twist from the oximato bridges presages an overall antiferromagnetic behavior for complex **1** (*vide infra*) [10,25,36]. Finally, one acetato O-atom from each triangle **B** becomes η^2:μ-bridging and serves to link the {Mn$^{III}_3$O(O$_2$CMe)$_3$(shi)$_2$}$^{2-}$ subunits with their symmetry-related ones. In addition, the oximato O-atoms of shi^{3-} ligands within **B** are further bridged to the Mn^{II} atoms (Mn1 and Mn5). Thus, complex **1** has an overall [Mn$^{II}_2$Mn$^{III}_9$(μ$_3$-O)$_4$(μ-OR)$_3$(μ$_3$-NO)$_6$]$^{14+}$ core (Fig. 3), where the RO$^-$ belongs to the monoatomic bridge of the MeCO$_2^-$ groups. The coordination modes of all the ligands present in complex **1** are depicted in Fig. 4.

Charge-balance considerations and an inspection of the metric parameters indicate a 2Mn^{II}, 9Mn^{III} description for **1**. This was confirmed quantitatively by bond valence sum (BVS) [37] calculations (Table 3), which identified Mn1 and Mn5 as the Mn^{II} ions, and the others as Mn^{III}. Six of the Mn^{III} atoms (Mn2, Mn3 and their symmetry-related partners) exhibit Jahn-Teller (JT) distortion, as expected for high-spin d^4 ions in near-octahedral geometry, taking the form of axial elongation of the two *trans* Mn-O$_{acetate}$ bonds. Thus, as is almost always the case, the JT elongation axes avoid the Mn^{III}-O^{2-} bonds, the shortest and strongest in the molecule [38]. The remaining three Mn^{III} atoms (Mn4 and their

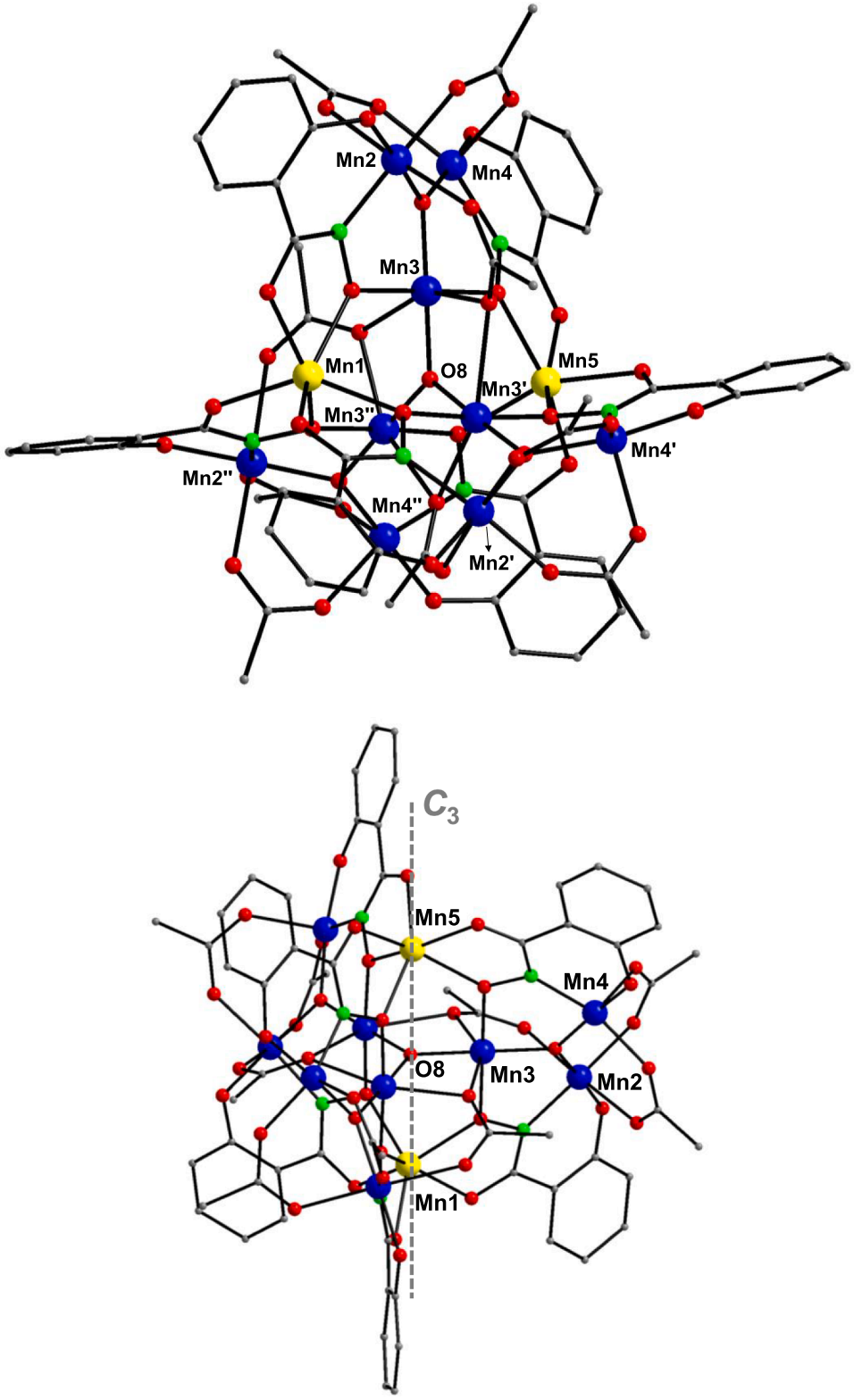

Fig. 1. Partially labeled representation of the anion of complex **1** (top), and a different view of its structure along the C_3-axis (bottom). H atoms are omitted for clarity. Color scheme: Mn^{II} yellow; Mn^{III} blue; O red; N green; C gray. Symmetry codes: (′) 1-*x*, 0.5 + *y*, 0.5-*z*; (″) −0.5 + *x*, 0.5-*y*, 1-*z*.

symmetry-equivalent atoms) are five-coordinate with distorted square pyramidal geometries. This was confirmed by analysis of the shape-determining bond angles using the approach of Reedijk and Addison [39], which yields a value for the trigonality index, τ, of 0.28 for the three metal ions, where τ is 0 and 1 for perfect square pyramidal and trigonal bipyramidal geometries, respectively.

Interestingly, the six-coordinate Mn^{II} atoms, Mn1 and Mn5, adopt an almost ideal trigonal prismatic and a very distorted octahedral geometry, respectively. This was confirmed by the Continuous Shape Measure (CShM) approach of the SHAPE program, which allows one to

Table 2
Selected interatomic distances (Å) and angles (°) for complex **1**·3MeCN.[a]

Bond lengths			
Mn(1)-O(1)	2.148(4)	Mn(3)-O(8)	1.856(4)
Mn(1)-O(1′)	2.148(4)	Mn(3)-O(13)	2.213(4)
Mn(1)-O(1″)	2.148(4)	Mn(3)-O(13″)	2.441(4)
Mn(1)-O(2)	2.212(4)	Mn(4)-O(6)	1.852(4)
Mn(1)-O(2′)	2.212(4)	Mn(4)-O(7)	1.854(4)
Mn(1)-O(2″)	2.212(4)	Mn(4)-O(10)	1.971(4)
Mn(2)-O(3)	1.862(4)	Mn(4)-O(12)	2.088(4)
Mn(2)-O(7)	1.871(4)	Mn(4)-N(2)	1.979(5)
Mn(2)-O(9)	2.222(4)	Mn(5)-O(4)	2.150(4)
Mn(2)-O(11)	1.978(4)	Mn(5)-O(4′)	2.150(4)
Mn(2)-O(14)	2.286(4)	Mn(5)-O(4″)	2.150(4)
Mn(2)-N(1)	1.971(5)	Mn(5)-O(5)	2.196(4)
Mn(3)-O(2)	1.918(4)	Mn(5)-O(5′)	2.196(4)
Mn(3)-O(5)	1.914(4)	Mn(5)-O(5″)	2.196(4)
Mn(3)-O(7)	1.867(4)		
Bond angles			
Mn(1)-O(2)-Mn(3)	124.8(2)	Mn(3)-O(5)-Mn(5)	121.8(2)
Mn(1)-O(2″)-Mn(3″)	124.8(2)	Mn(3)-O(13)-Mn(3′)	87.2(1)
Mn(2)-O(7)-Mn(3)	114.4(2)	Mn(3)-O(8)-Mn(3′)	120.0(1)
Mn(2)-O(7)-Mn(4)	126.5(2)	Mn(3)-O(8)-Mn(3″)	120.0(1)
Mn(3)-O(7)-Mn(4)	118.8(2)	Mn(3′)-O(8)-Mn(3″)	120.0(1)
Torsion angles			
Mn(2)-N(1)-O(2)-Mn(3)	3.2(4)	Mn(4)-N(2)-O(5)-Mn(3)	21.2(4)
Mn(2)-N(1)-O(2)-Mn(1)	160.9(2)	Mn(4)-N(2)-O(5)-Mn(5)	176.9(2)

[a] Symmetry codes: (′) 1-*x*, 0.5 + *y*, 0.5-*z*; (″) −0.5 + *x*, 0.5-*y*, 1-*z*.

Table 3
Bond valence sum (BVS)[a,b] calculations for Mn and selected O atoms in **1**.

Atom	Mn^{II}	Mn^{III}	Mn^{IV}
Mn1	1.96	1.79	1.88
Mn2	3.33	3.09	3.18
Mn3	3.33	3.05	3.20
Mn4	3.27	3.03	3.12
Mn5	2.00	1.83	1.92
	BVS	assignment	
O7	2.00	O^{2-} (μ_3)	
O8	2.05	O^{2-} (μ_3)	

[a] The underlined value is the one closest to the charge for which it was calculated. The oxidation state is the nearest whole number to the underlined value. [b] An O BVS in the ~1.7–2.0, ~1.0–1.2, and ~0.2–0.4 ranges is indicative of non–, single- and double-protonation, respectively.

numerically evaluate by how much a particular geometry deviates from an ideal shape [40]. The best fit for Mn1 was obtained for the trigonal prism with CShM value of 1.89 and the octahedron for Mn5 with CShM value of 4.55 (Fig. 5). Values of CShM between 0.1 and 3 usually correspond to a non-negligible but still small distortion from ideal geometry [41]. Undoubtedly, Mn1 adopts a trigonal prismatic geometry, with the second closest CShM value being that of the octahedron (CShM = 10.81). The large difference between the CShM values for the trigonal prism vs. octahedron indicates the superior preference of Mn1 for the trigonal prismatic geometry. The three symmetry-related O(1,1′,1″) and O(2,2′,2″) atoms from the alkoxido and oximato parts of the shi^{3-} ligands, respectively, constitute the two trigonal faces. The

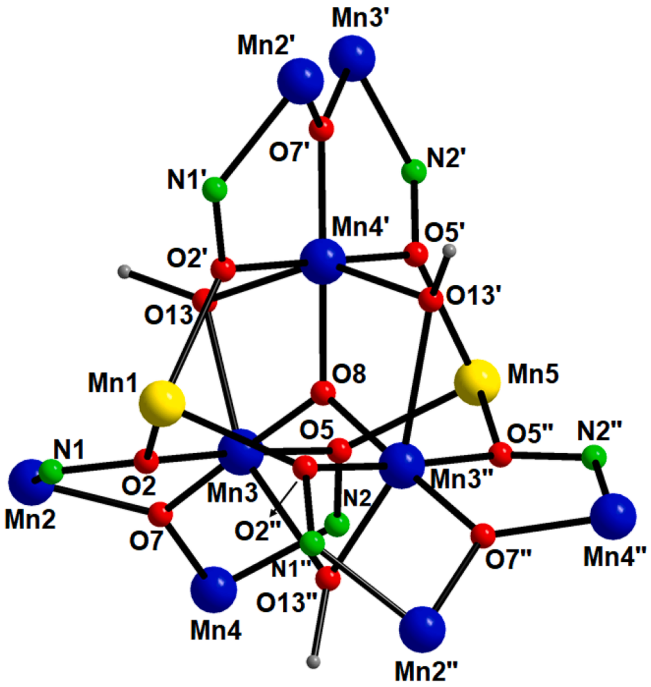

Fig. 3. Labeled representation of the complete $[Mn^{II}_2Mn^{III}_9(\mu_3\text{-}O)_4(\mu\text{-}OR)_3(\mu_3\text{-}NO)_6]^{14+}$ core of **1**. Color scheme and symmetry codes as in Fig. 1.

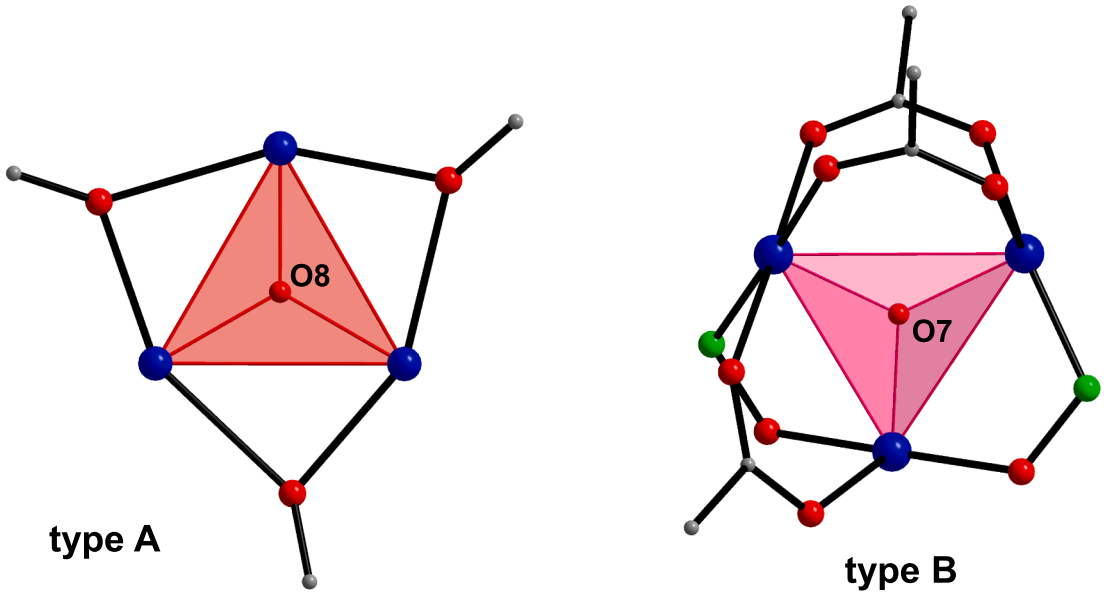

Fig. 2. Representation of the two types of triangular subunits present in the structure of complex **1**. Color scheme as in Fig. 1.

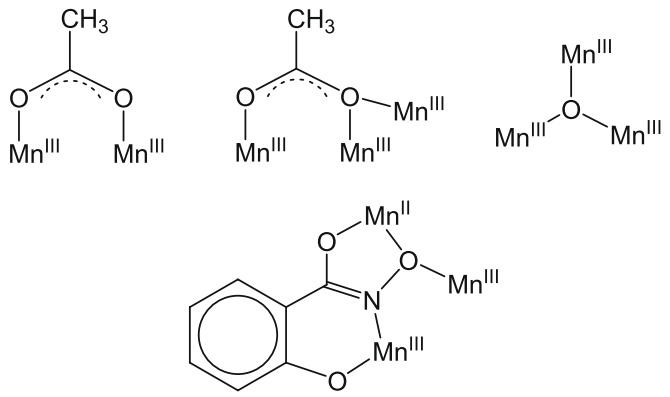

Fig. 4. Coordination modes of all the ligands present in the structure of **1**.

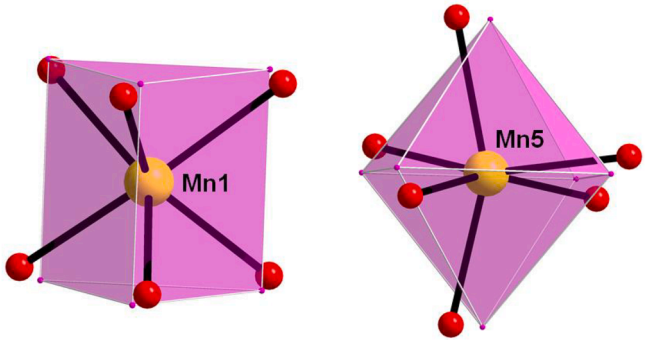

Fig. 5. Trigonal prismatic (left) and distorted octahedral (right) coordination geometries of the Mn1 and Mn5 atoms, respectively, in **1**. Points connected by the white thin lines define the vertices of the ideal polyhedral, as derived from the use of the program SHAPE. Color scheme as in Fig. 1.

latter are perfectly parallel, the planes defined by O1-O1′-O1″ and O2-O2′–O2″ forming an angle of 0°. All three tetragonal faces are irregular trapezoids. For Mn5, the case is very different, and the second closest CShM value was calculated as 6.93 for a trigonal prismatic geometry. This implies a significant distortion of the Mn5 polyhedron from the ideal octahedron or trigonal prismatic shape. Finally, the protonation level of O^{2-} groups was also confirmed by BVS calculations (Table 3).

From a supramolecular perspective, the {Mn_{11}} clusters appear to be well-separated from each other in the crystal due to the presence of the Me_4N^+ countercations and the lattice MeCN molecules. Neither H-bonding interactions nor any other secondary interaction (i.e., π-π stacking) appear to significantly affect the communication of the cluster compounds in the crystal. Finally, the space-filling representation (Fig. 6) shows that **1** adopts a nanosized, nearly spherical motif with dimensions of ~1.6 and ~1.8 nm, as defined by the longest C—H···H—C distances.

Complex **1** joins only a handful of previous manganese clusters with a nuclearity of 11. Since most of these were reported only relatively recently, we have listed them in Table 4 for a convenient comparison of their formulae, oxidation states description, and pertinent magnetic data such as their ground state spin (*S*) values and the nature of predominant magnetic exchange interactions. The combined examination of Table 4 and the previously reported in literature results show that **1** has a similar core topology with the complexes {$Na_4[Mn_{11}O_4(O_2CMe)_9(shi)_6(DMF)_3]$}$_n$, {$Na_{3.5}H_{0.5}[Mn_{11}O_4(O_2CMe)_9(p\text{-}ashi)_6]$}$_n$ and {$H[Mn_{11}O_4(OH)_3(O_2CMe)_3(p\text{-}pyshi)_6]$}$_n$ but not the same chemical formula (i.e., different countercations and coordinating ligands) or structural conformation (0-D vs. 3-D). Complex **1** is a discrete 0-D cluster and its complete magnetic study (*vide infra*) allows us to: (a) evaluate the nature of the predominant magnetic exchange interactions between the metal centers, (b) determine the ground state spin value for such a core topology, and (c) explore whether it is an SMM or not.

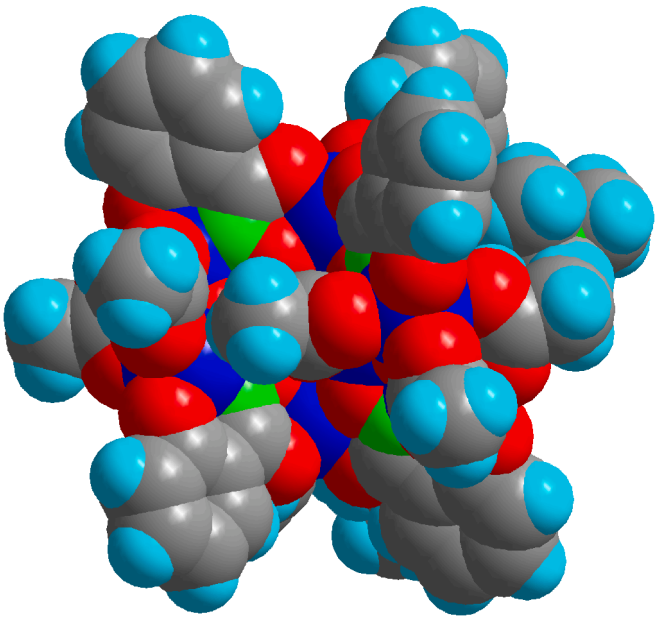

Fig. 6. Space-filling representation of the anion of **1**. Color scheme as in Fig. 1. H atoms are shown in cyan.

3.3. Magnetic susceptibility studies

Variable-temperature dc magnetic susceptibility measurements were performed on a powdered microcrystalline sample of **1**·3H_2O, in a 1 kG (0.1 T) field and in the 5.0–300 K range. The obtained data are shown as a $\chi_M T$ vs. *T* plot in Fig. 7. The $\chi_M T$ product steadily decreases from 27.12 cm^3Kmol^{-1} at 300 K to 14.39 cm^3Kmol^{-1} at 50 K, and then it rapidly drops further to 5.99 cm^3Kmol^{-1} at 5.0 K. The $\chi_M T$ value at 300 K is much less than the spin-only ($g = 2$) value of 35.75 cm^3Kmol^{-1} for two Mn^{II} (d^5; $S = 5/2$) and nine Mn^{III} (d^4; $S = 2$) non-interacting ions, indicating the presence of dominant antiferromagnetic exchange interactions and a low, but possibly non-zero, ground state *S* value. In fact, the $\chi_M T$ at 5 K indicates that complex **1** possesses an $S = 3$ spin ground state; the spin-only ($g = 2$) value for an $S = 3$ is 6.0 cm^3Kmol^{-1}, in agreement with the recorded experimental data of **1**.

To determine the spin ground state of the complex, magnetization data were collected in the magnetic field and temperature ranges of 1–70 kG and 1.8–10.0 K, respectively. However, we could not get an acceptable fit using data collected over the entire field range, which is a common problem caused by low-lying excited states, especially if some have an *S* value greater than that of the ground state, as is the case for **1** on the basis of Fig. 7. A common solution to overcome this problem is to only use data collected with low fields (≤1.0 T, inset of Fig. 7), as we previously reported for many mixed-valence Mn^{II}/Mn^{III} clusters [46]. However, it was still not possible to obtain a satisfactory fit assuming that only the ground state is populated in this temperature range. This suggests that low-lying excited states are still populated, even at these relatively low temperatures, mainly because of the weak magnetic coupling within the $Mn^{II}\cdots Mn^{III}$ and $Mn^{III}\cdots Mn^{III}$ pairs [47].

As has been described in several previous cases [48], ac magnetic susceptibility studies provide a powerful complement to dc studies for determining the ground state of a system because they preclude complications arising from the presence of a dc field. Therefore, ac susceptibility measurements were carried out for **1** in a 3.5 G ac field oscillating at frequencies in the 50–1000 Hz range to determine both the ground state spin, *S*, and whether **1** exhibits slow magnetization relaxation and

Table 4
Chemical formulae, oxidation states description, ground-state S values, and nature of magnetic exchange interactions for polynuclear Mn complexes with a nuclearity of 11.

Complex[a,b]	Oxidation states	S	Magnetic interactions	Refs.
$[Mn_{11}O_{10}Cl_2(O_2CMe)_{11}(bpy)_2(MeCN)_2(H_2O)_2](ClO_4)_2$	$Mn^{III}_9Mn^{IV}_2$	n.r.	n.r.	[42]
$[Mn_{11}O_2(OH)_2(nmpd)(pdmH)_5(pdm)_5Cl_6]$	$Mn^{II}_4Mn^{III}_7$	10	F (non-SMM)	[43]
$[Mn_{11}O_{12}(O_2CPh)_{15}]$	$Mn^{III}_5Mn^{IV}_6$	5	AF (SMM)	[44]
$[Mn_{11}O_7(OMe)_7(O_2CPh)_7(dphmp)_4(MeOH)_2]$	$Mn^{II}Mn^{III}_{10}$	5/2	AF (SMM)	[45]
$\{Na_4[Mn_{11}O_4(O_2CMe)_9(shi)_6(DMF)_3]\}_n$	$Mn^{II}_2Mn^{III}_9$	n.r.	n.r.	[35]
$\{Na_{3.5}H_{0.5}[Mn_{11}O_4(O_2CMe)_9(p\text{-}ashi)_6]\}_n$	$Mn^{II}_2Mn^{III}_9$	n.r.	n.r.	[35]
$\{H[Mn_{11}O_4(OH)_3(O_2CMe)_3(p\text{-}pyshi)_6]\}_n$	$Mn^{II}_2Mn^{III}_9$	n.r.	n.r.	[35]
$(Me_4N)_4[Mn_{11}O_4(O_2CMe)_9(shi)_6]$	$Mn^{II}_2Mn^{III}_9$	3	AF (non-SMM)	t.w.

[a] Lattice solvate molecules are omitted.
Abbreviations: F = ferromagnetic, AF = antiferromagnetic, n.r. = not reported, t.w. = this work, bpy = 2,2′-bipyridine, $nmpdH_2$ = 2-nitro-2-methyl-1,3-propanediol, $pdmH_2$ = pyridine-2,6-dimethanol, dphmpH = diphenyl(pyridine-2-yl)methanol, DMF = N,N-dimethylformamide, p-$ashiH_3$ = 4-aminosalicylhydroxamic acid, p-$pyshiH_3$ = 4-(pyridin-4-yl)-salicylhydroxamic acid.

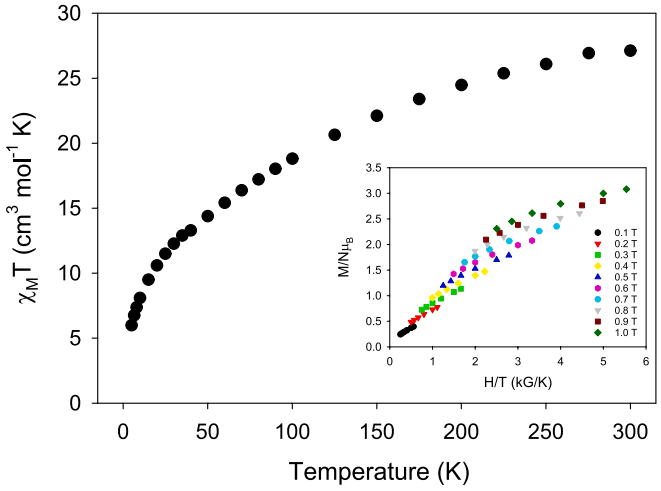

Fig. 7. Plot of $\chi_M T$ vs. T for **1**·3H_2O in a 1 kG field. (inset) Reduced magnetization plot of $M/N\mu_B$ vs. H/T for **1**·3H_2O at the indicated applied fields.

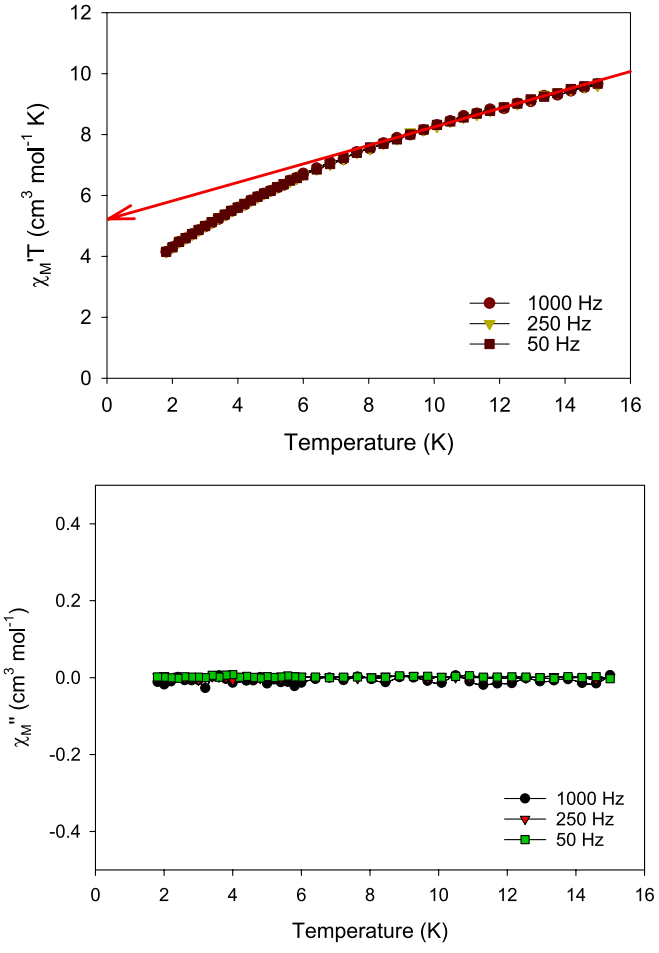

Fig. 8. Plots of the: (top) in-phase (χ'_M) (as $\chi'_M T$), and (bottom) out-of-phase (χ''_M) ac susceptibility signals for **1**·3H_2O, measured in a 3.5 G field oscillating at the indicated frequencies. The red solid line indicates the data used to determine the spin ground state, S, of **1** (see the discussion in the text).

SMM behavior. If the magnetization vector can relax fast enough to keep up with the oscillating field, then there is no imaginary (out-of-phase) susceptibility signal (χ''_M), and the real (in-phase) susceptibility (χ'_M) is equal to the dc susceptibility [49]. The $\chi'_M T$ extrapolated from a temperature high enough to avoid the effects of any weak intermolecular interactions or slow relaxation to 0 K (where only the ground state would be populated) should thus be in agreement with the formula $\chi'_M T = g^2 S(S+1)/8$, where S is the ground state of the compound. However, if the barrier to magnetization relaxation is significant compared to the thermal energy (kT), then there is a non-zero χ''_M signal and the in-phase signal decreases. In addition, the χ''_M signal will be frequency-dependent. Such frequency-dependent χ''_M signals are a characteristic signature of the superparamagnetic-like properties of an SMM (but by themselves do not prove the presence of an SMM [50]).

For complex **1**, the in-phase signal (plotted as $\chi'_M T$ vs. T, Fig. 8, top) decreases almost linearly from ~9.6 cm^3Kmol^{-1} at 15 K to ~6.7 cm^3Kmol^{-1} at 6 K, followed by a further drop until 1.8 K. The observed decrease of the $\chi'_M T$ values at the higher T region (>6 K) is due to depopulation of excited states with spin S larger than that of the ground state, while the very low-T drop of the $\chi'_M T$ could be also affected by any weak intermolecular interactions and/or zero-field splitting. Extrapolation of $\chi'_M T$ to 0 K using the data above 6 K (red line in Fig. 8, top) gives a value of ~5.4 cm^3Kmol^{-1}, indicative of a spin ground state of $S = 3$ with g slightly less than 2.0, in good agreement with the conclusions derived from the dc studies. Unfortunately, and not surprisingly due to the small S value, complex **1** does not show any frequency-dependent out-of-phase ac signals down to 1.8 K (Fig. 8, bottom), i.e. it is not an SMM.

An $S = 3$ ground state for a $2Mn^{II}$, $9Mn^{III}$ complex such as **1** that has spin values in the $S = 0$–23 range is consistent with predominant antiferromagnetic coupling and the presence of spin frustration effects arising from the antiferromagnetic coupling within the several triangular units in the structure. There are thus various possible coupling schemes and resulting intermediate spin alignments at some metals that could yield an $S = 3$ ground state, rendering it difficult to rationalize the

observed value in a unique manner without recourse to theoretical calculations.

4. Conclusions and perspectives

The present work extends the body of results that emphasize the ability of salicylhydroxamic acid ($shaH_2$) to yield interesting structural types in Mn cluster chemistry with rare nuclearities and aesthetically pleasing topologies. In addition to the recently reported $\{Na_4[Mn_{11}O_4(O_2CMe)_9(shi)_6(DMF)_3]\}_n$, $\{Na_{3.5}H_{0.5}[Mn_{11}O_4(O_2CMe)_9(p\text{-}ashi)_6]\}_n$ and $\{H[Mn_{11}O_4(OH)_3(O_2CMe)_3(p\text{-}pyshi)_6]\}_n$ multidimensional polymers-of-clusters [35], the $Mn/MeCO_2^-/shaH_2$ reaction system has provided further access to the discrete undecanuclear 0-D compound $(Me_4N)_4[Mn_{11}O_4(O_2CMe)_9(shi)_6]$ (**1**), in the presence of base Me_4NOH. The combined results also demonstrate the ability of shi^{3-} to stabilize Mn/O^{2-} cores, a relatively rare case given the usual trend of shi^{3-} to yield oxido-free metallacrowns. The predominant antiferromagnetic exchange interactions between the metal centers within the structurally different, vertex-sharing triangular subunits lead to a small, but nonzero, ground state spin value of $S = 3$ for **1**.

We are currently investigating how the replacement of $MeCO_2^-$ groups by various other carboxylate ions, less employed before in Mn cluster chemistry, may affect the structural identity and/or the magnetic properties of the resulting Mn/shi^{3-} products, and to what extent this might prove a route to new cluster types, high-spin molecules and SMMs.

Declaration of Competing Interest

The authors declare that they have no known competing financial interests or personal relationships that could have appeared to influence the work reported in this paper.

Acknowledgements

This research is co-financed by Greece and the European Union (European Social Fund - ESF) through the Operational Programme "Human Resources Development, Education and Lifelong Learning 2014-2020" in the context of the project "New Families of Molecular Ferromagnetic Materials with Implications in Molecular Electronics and Spintronics" (MIS 5047176). A.J.T acknowledges the Cyprus Research and Innovation Foundation Research Grant "EXCELLENCE/1216/0076" which is co-funded by the Republic of Cyprus and the European Regional Development Fund. G.C. thanks the U.S. National Science Foundation (Grant CHE-1900321) for support.

Appendix A. Supplementary data

Supplementary data to this article can be found online at https://doi.org/10.1016/j.poly.2021.115298.

References

[1] C. Papatriantafyllopoulou, E.E. Moushi, G. Christou, A.J. Tasiopoulos, Chem. Soc. Rev. 45 (2016) 1597.
[2] (a) G. Christou, Polyhedron 24 (2005) 2065.(b) R. E. P. Winpenny, in *Comprehensive Coordination Chemistry II*, ed. J. A. McCleverty and T. J. Meyer, Elsevier, Amsterdam, 2004, vol. 7, pp. 125-175.
[3] P.S. Perlepe, D. Maniaki, E. Pilichos, E. Katsoulakou, S.P. Perlepes, Inorganics 8 (2020) 39.
[4] X.-Y. Zheng, J. Xie, X.-J. Kong, L.-S. Long, L.-S. Zheng, Coord. Chem. Rev. 378 (2019) 222.
[5] H.L.C. Feltham, S. Brooker, Coord. Chem. Rev. 276 (2014) 1.
[6] (a) T.C. Stamatatos, K.A. Abboud, W. Wernsdorfer, G. Christou, Angew. Chem. Int. Ed. 46 (2007) 884;
(b) M. Murugesu, M. Habrych, W. Wernsdorfer, K.A. Abboud, G. Christou, J. Am. Chem. Soc. 126 (2004) 4766;
(c) T.C. Stamatatos, K.A. Abboud, W. Wernsdorfer, G. Christou, Angew. Chem. Int. Ed. 45 (2006) 4134;
(d) T.C. Stamatatos, K.A. Abboud, W. Wernsdorfer, G. Christou, Angew. Chem. Int. Ed. 47 (2008) 6694.
[7] (a) A.J. Tasiopoulos, S.P. Perlepes, Dalton Trans. (2008) 5537;
(b) E.K. Brechin, Chem. Commun. (2005) 5141.
[8] (a) M. Andruh, Dalton Trans. 44 (2015) 16633;
(b) M. Gebrezgiabher, Y. Bayeh, T. Gebretsadik, G. Gebreslassie, F. Elemo, M. Thomas, W. Linert, Inorganics 8 (2020) 66.
[9] (a) C.J. Milios, T.C. Stamatatos, S.P. Perlepes, Polyhedron 25 (2006) 134;
(b) T.C. Stamatatos, D. Foguet-Albiol, S.-C. Lee, C.C. Stoumpos, C.P. Raptopoulou, A. Terzis, W. Wernsdorfer, S.O. Hill, S.P. Perlepes, G. Christou, J. Am. Chem. Soc. 129 (2007) 9484.
[10] C.J. Milios, S. Piligkos, E.K. Brechin, Dalton Trans. (2008) 1809.
[11] (a) D.I. Alexandropoulos, K.M. Poole, L. Cunha-Silva, J. Ahmad Sheikh, W. Wernsdorfer, G. Christou, T.C. Stamatatos, Chem. Commun. 53 (2017) 4266;
(b) A.A. Alaimo, A. Worrell, S. Das Gupta, K.A. Abboud, C. Lampropoulos, G. Christou, T.C. Stamatatos, Chem. Eur. J. 24 (2018) 2588.
[12] (a) G.S. Papaefstathiou, S.P. Perlepes, Comments Inorg. Chem. 23 (2002) 249;
(b) A.A. Athanasopoulou, M. Pilkington, C.P. Raptopoulou, A. Escuer, T. C. Stamatatos, Chem. Commun. 50 (2014) 14942.
[13] Th. C. Stamatatos, C. G. Efthymiou, C. C. Stoumpos, S. P. Perlepes, Eur. J. Inorg. Chem. (2009) 3361 (Microreview).
[14] A. Escuer, J. Esteban, S.P. Perlepes, T.C. Stamatatos, Coord. Chem. Rev. 275 (2014) 87.
[15] (a) S. Mukherjee, J.A. Stull, J. Yano, T.C. Stamatatos, K. Pringouri, T.A. Stich, K. A. Abboud, R.D. Britt, V.K. Yachandra, G. Christou, Proc. Natl. Acad. Sci. 109 (2012) 2257;
(b) B. Gerey, E. Gouré, J. Fortage, J. Pécaut, M.-N. Collomb, Coord. Chem. Rev. 319 (2016) 1;
(c) C. Zhang, C. Chen, H. Dong, J.-R. Shen, H. Dau, J.A. Zhao, Science 348 (2015) 690;
(d) J.S. Kanady, E.Y. Tsui, M.W. Day, T.A. Agapie, Science 333 (2011) 733.
[16] For a comprehensive review, see: R. Bagai, G. Christou, Chem. Soc. Rev. 38 (2009) 1011.
[17] S. Nayak, M. Evangelisti, A.K. Powell, J. Reedijk, Chem. Eur. J. 16 (2010) 12865.
[18] (a) D.I. Alexandropoulos, A.M. Mowson, M. Pilkington, V. Bekiari, G. Christou, T. C. Stamatatos, Dalton Trans. 43 (2014) 1965;
(b) C.-M. Liu, R.-G. Xiong, D.-Q. Zhang, D.-B. Zhu, J. Am. Chem. Soc. 132 (2010) 4044.
[19] G. Maayan, N. Gluz, G. Christou, Nature Catalysis 1 (2018) 48.
[20] A.J. Tasiopoulos, A. Vinslava, W. Wernsdorfer, K.A. Abboud, G. Christou, Angew. Chem. Int. Ed. 43 (2004) 2117.
[21] A. Vinslava, A.J. Tasiopoulos, W. Wernsdorfer, K.A. Abboud, G. Christou, Inorg. Chem. 55 (2016) 3419.
[22] M. Manoli, S. Alexandrou, L. Pham, G. Lorusso, W. Wernsdorfer, M. Evangelisti, G. Christou, A.J. Tasiopoulos, Angew. Chem. Int. Ed. 55 (2016) 679.
[23] For example, see: A. A. Alaimo, D. Takahashi, L. Cunha-Silva, G. Christou, Th. C. Stamatatos, Inorg. Chem. 54 (2015) 2137.
[24] (a) M.S. Lah, V.L. Pecoraro, J. Am. Chem. Soc. 111 (1989) 7258;
(b) B.R. Gibney, H. Wang, J.W. Kampf, V.L. Pecoraro, Inorg. Chem. 35 (1996) 6184.
[25] (a) E.S. Koumousi, S. Mukherjee, C.M. Beavers, S.J. Teat, G. Christou, T. C. Stamatatos, Chem. Commun. 47 (2011) 11128;
(b) A.A. Alaimo, E.S. Koumousi, L. Cunha-Silva, L.J. McCormick, S.J. Teat, V. Psycharis, C.P. Raptopoulou, S. Mukherjee, C.R. Li, S. Das Gupta, A. Escuer, G. Christou, T.C. Stamatatos, Inorg. Chem. 56 (2017) 10760.
[26] (a) C.M. Zaleski, J.W. Kampf, T. Mallah, M.L. Kirk, V.L. Pecoraro, Inorg. Chem. 46 (2007) 1954;
(b) T.T. Boron, J. Lutter, C.I. Daly, C.Y. Chow, A. Davis, A. Nimthong-Roldan, M. Zeller, J. Kampf, C.M. Zaleski, V.L. Pecoraro, Inorg. Chem. 55 (2016) 10597.
[27] For an excellent review, see: V. L. Pecoraro, A. J. Stemmler, B. R. Gibney, J. J. Bodwin, H. Wang, J. W. Kampf, A. Barwinski, Prog. Inorg. Chem. 45 (1997) 83.
[28] G.A. Bain, J.F. Berry, J. Chem. Educ. 85 (2008) 532.
[29] CrysAlis CCD and CrysAlis RED. Oxford Diffraction Ltd.: Abingdon, U.K. (2008).
[30] G.M. Sheldrick, Acta Crystallogr., Sect. A: Found. Crystallogr. A64 (2008) 112.
[31] L.J. Farrugia, J. Appl. Crystallogr. 45 (2012) 849.
[32] G.M. Sheldrick, A. Crystallogr, C. Sect, Struct. Chem. C71 (2015) 3.
[33] C.B. Hübschle, G.M. Sheldrick, B. Dittrich, J. Appl. Crystallogr. 44 (2011) 1281.
[34] K. Bradenburg, DIAMOND, Release 3.1f, Crystal Impact GbR; Bonn, Germany (2008).
[35] V. Marzaroli, G. Spigolon, G. Lococciolo, M. Quaretti, C. Salviati, J.W. Kampf, G. Licini, L. Marchio, V.L. Pecoraro, M. Tegoni, Cryst. Growth Des. 19 (2019) 1954.
[36] Th. C. Stamatatos, D. Foguet-Albiol, C. C. Stoumpos, C. P. Raptopoulou, A. Terzis, W. Wernsdorfer, S. P. Perlepes, G. Christou, J. Am. Chem. Soc. 127 (2005) 15380.
[37] (a) W. Liu, H.H. Thorp, Inorg. Chem. 32 (1993) 4102;
(b) I.D. Brown, D. Altermatt, Acta Crystallogr. Sect. B (1985) 244.
[38] (a) N.E. Chakov, S.-C. Lee, A.G. Harter, P.L. Kuhns, A.P. Reyes, S.O. Hill, N. S. Dalal, W. Wernsdorfer, K.A. Abboud, G. Christou, J. Am. Chem. Soc. 128 (2006) 6975;
(b) T.C. Stamatatos, B.S. Luisi, B. Moulton, G. Christou, Inorg. Chem. 47 (2008) 1134.
[39] A. W. Addison, T. N. Rao, J. Reedijk, J. van Rijn, G. C. Verschoor, J. Chem. Soc., Dalton Trans. (1984) 1349.
[40] H. Zabrodsky, S. Peleg, D. Avnir, J. Am. Chem. Soc. 115 (1993) 8278.
[41] (a) S. Alvarez, P. Alemany, D. Casanova, J. Cirera, M. Llunell, D. Avnir, Coord. Chem. Rev. 249 (2005) 1693;
(b) H. Zabrodsky, S. Peleg, D. Avnir, J. Am. Chem. Soc. 114 (1992) 7843.

[42] S.P. Perlepes, J.C. Huffman, G. Christou, J. Chem. Soc., Chem. Commun. (1991) 1657.
[43] M. Murugesu, W. Wernsdorfer, K.A. Abboud, G. Christou, Polyhedron 24 (2005) 2894.
[44] T.C. Stamatatos, A. Vinslava, K.A. Abboud, G. Christou, Chem. Commun. (2009) 2839.
[45] T. Taguchi, M.R. Daniels, K.A. Abboud, G. Christou, Inorg. Chem. 48 (2009) 9325.
[46] (a) P. King, W. Wernsdorfer, K.A. Abboud, G. Christou, Inorg. Chem. 44 (2005) 8659;
(b) A.J. Tasiopoulos, W. Wernsdorfer, K.A. Abboud, G. Christou, Inorg. Chem. 44 (2005) 6324.
[47] T.C. Stamatatos, G. Christou, Phil. Trans. R. Soc. A 366 (2008) 113.
[48] (a) T.C. Stamatatos, D. Foguet-Albiol, W. Wernsdorfer, K.A. Abboud, G. Christou, Chem. Commun. 47 (2011) 274;
(b) T.C. Stamatatos, K.A. Abboud, G. Christou, Polyhedron 28 (2009) 1880;
(c) D.I. Alexandropoulos, C. Papatriantafyllopoulou, G. Aromi, O. Roubeau, S. J. Teat, S.P. Perlepes, G. Christou, T.C. Stamatatos, Inorg. Chem. 49 (2010) 3962;
(d) D.I. Alexandropoulos, E.C. Mazarakioti, S.J. Teat, T.C. Stamatatos, Polyhedron 64 (2013) 91.
[49] M. A. Novak, R. Sessoli, In Quantum Tunnelling of Magnetization, QTM'94; L. Gunther, B. Barbar, Eds.; Kluwer: Dordrecht, The Netherlands (1995); pp 171-188.
[50] (a) N.E. Chakov, W. Wernsdorfer, K.A. Abboud, G. Christou, Inorg. Chem. 43 (2004) 5919;
(b) A. Mishra, A.J. Tasiopoulos, W. Wernsdorfer, K.A. Abboud, G. Christou, Inorg. Chem. 46 (2007) 3105.